Atmos. Meas. Tech. Discuss., https://doi.org/10.5194/amt-2018-388
Manuscript under review for journal Atmos. Meas. Tech.
Discussion started: 24 January 2019

Atmospheric Measurement Techniques
Discussions
Open Access
EGU

Estimation of Liquid Water Path in Stratiform Precipitation Systems using Radar Measurements during MC3E

Jingjing Tian[1], Xiquan Dong[1], Baike Xi[1], Christopher R. Williams[2], and Peng Wu[1]

[1]Department of Hydrology and Atmospheric Sciences, University of Arizona, Tucson, Arizona, USA

[2] Department of Ann and H.J. Smead Aerospace Engineering Sciences, University of Colorado Boulder

Manuscript Submitted to Atmospheric Measurement Techniques

Corresponding author address: Dr. Xiquan Dong, The Department of Hydrology and Atmospheric Sciences, University of Arizona, 1133 E. James Rogers Way, Tucson, AZ 85721-0011.

Email: xdong@email.arizona.edu; Phone: 520-621-4652

Abstract

In this study, the liquid water path (LWP) in stratiform precipitation systems is retrieved, which is a combination of rain liquid water path (RLWP) and cloud liquid water path (CLWP). The retrieval algorithm uses measurements from the vertically pointing radars (VPRs) at 35 GHz and 3 GHz operated by the U.S Department of Energy Atmospheric Radiation Measurement (ARM) and National Oceanic and Atmospheric Administration (NOAA) during the field campaign Midlatitude Continental Convective Clouds Experiment (MC3E). The measured radar reflectivity and mean Doppler velocity from both VPRs and spectrum width from the 35 GHz radar are utilized. With the aid of the cloud base detected by ceilometer, the LWP in the liquid layer is retrieved under two different situations: (I) no cloud exists below the melting base, and (II) cloud exists below the melting base. In (I), LWP is primarily contributed from raindrops only, i.e., RLWP, which is estimated by analyzing the Doppler velocity differences between two VPRs. In (II), cloud particles and raindrops coexist below the melting base. The CLWP is estimated using a modified attenuation-based algorithm. Two stratiform precipitation cases (20 May 2011 and 11 May 2011) during MC3E are illustrated for two situations, respectively. With a total of 14 hours of samples during MC3E, statistical results show that the occurrence of cloud particles below the melting base is low (8%), however, the mean CLWP value can be up to 0.87 kg m^{-2}, which is much larger than the RLWP (0.22 kg m^{-2}). When only raindrops exist below the melting base, the averaged RLWP value is larger (0.33 kg m^{-2}) than the with cloud situation. The overall mean LWP below the melting base is 0.39 kg m^{-2} for stratiform systems during MC3E.

1. Introduction

Clouds in stratiform precipitation systems are important to the Earth's radiation budget. The vertical distributions of cloud microphysics, ice and liquid water content (IWC/LWC), determine the surface and top-of-the-atmosphere radiation budget and redistribute energy in the atmosphere (Feng et al., 2011; 2018). Also, stratiform precipitation systems are responsible for most tropical and midlatitude precipitation during summer (Xu, 2013). However, the representation of those systems in global climate and cloud-resolving models are still challenging (Fan et al., 2015). One of the challenges is due to the lack of comprehensive observations and retrievals of cloud microphysics (e.g. prognostic variables IWC and LWC) in stratiform precipitation systems. Liquid water path (LWP), defined as an integral of LWC in the atmosphere. It is a parameter used to provide the characterization of liquid hydrometeors in the vertical column of atmosphere and study clouds and precipitation. The estimation of LWC/LWP is one of the critical objectives of the US Department of Energy's (DOE) Atmospheric Radiation Measurement (ARM) Program (Ackerman and Stokes, 2003).

LWP can be retrieved using the ground-based MicroWave Radiometer (MWR) sensed downwelling radiant energy at 23.8 and 31.4 GHz (Liljegreen et al., 2001). In last two decades, ARM has been operating a network of 2-channel (23.8- and 31.4-GHz) ground-based MWR to provide a time series of LWP at the ARM Southern Great Plains (SGP) site (Cadeddu et al., 2013). Absorption-based algorithms using multichannels of MWRs have been widely used to retrieve cloud LWP (e.g., Liljegren et al. 2001; Turner, 2007), and it is known to be accurate methods to estimate LWP of nonprecipitating clouds with mean LWP error of 15 g m^{-2} (Crewell and Löhnert, 2003). However, in precipitating conditions, LWP retrieved from conventional

MWR are generally not valid due to the violation of the Rayleigh assumption when large raindrops exist (e.g., Saavedra et al., 2012). In addition, large increase of brightness temperatures is measured as a result of the deposition of raindrops on the MWR's radome. Unfortunately, it is very hard to model and quantify this increase from rain layer on the radome (Cadeddu et al., 2017). This "wet-radome" issue largely inhibits the retrieving of LWPs using ground-based MWR during precipitation. Due to the limitations of retrieving LWP from MWR during precipitation, cloud and precipitation radars were used to simultaneously retrieve LWP (Matrosov, 2010).

In the precipitating system, the liquid water cloud droplets and raindrops often coexist in the same atmospheric layer (e.g., Dubrovina, 1982; Mazin, 1989; Matrosov, 2009, 2010), indicating that the LWP consists of both cloud liquid water path (CLWP) and rain liquid water path (RLWP). However, the discrimination between suspended small cloud liquid water droplets and precipitating large raindrops is a very challenging remote sensing problem. Even though the partitioning of LWP into CLWP and RLWP is important in cloud modeling (Wentz and Spencer, 1998; Hillburn and Wentz, 2008), there are few studies retrieved RLWP and CLWP simultaneously and separately (Saavedra et al., 2012; Cadeddu et al., 2017). Battaglia et al. (2009) developed an algorithm to retrieve RLWP and CLWP from the six Advanced Microwave Radiometer for Rain Identification (ADMIRARI) observables under rainy conditions. Saavedra et al (2012) developed an algorithm using both ADMIRARI and a micro rain radar to retrieve and analyze the CLWP and RLWP for midlatitude precipitation during fall. In addition to these RLWP and CLWP estimations mainly from passive microwave radiometers, there are several studies to estimate the LWP using active radar measurements only. Ellis and Vivekanandan (2011) developed an attenuation-based technique to estimate LWC, which is the sum of cloud

Atmos. Meas. Tech. Discuss., https://doi.org/10.5194/amt-2018-388
Manuscript under review for journal Atmos. Meas. Tech.
Discussion started: 24 January 2019

water contents (CLWC) and rain liquid water contents (RLWC), using simultaneous S- and Ka-band scanning radars measurements. However, it is not always applicable of using these techniques to retrieve LWC. If raindrop diameters are comparable to at least one of the radars' wavelength, "Mie effect" will be included in the measured differential reflectivity, however this "Mie effect" is not very distinguishable from differential attenuation effects (Tridon et al., 2013; Tridon and Battaglia 2015).

Matrosov (2009) developed an algorithm to simultaneously retrieve CLWP and layer-mean rain rate using the radar reflectivity measurements from three ground-based W-, Ka-, S-bands radars. The CLWP were retrieved based on estimating the attenuation of cloud radar signals compared to S-band radar measurements. Matrosov (2010) developed an algorithm to estimate CLWP using a vertical pointing Ka-band radar and a nearby scanning C-band radar. The layer-mean rain rate was first estimated with the aid of surface disdrometer, and then CLWP was retrieved by subtracting the rain attenuation from total attenuation measured from two radars. For the estimation of RLWP, Williams et al. (2016) developed a retrieval algorithm for rain drop size distribution (DSD) using doppler spectrum moments observed from two collocated vertical pointing radar (VPRs) at frequencies of 3 GHz and 35 GHz. The retrieved air motion and DSD parameters were evaluated using the retrievals from a collocated 448-MHz VPR.

In this study, the CLWP retrieval algorithms in Matrosov (2009 and 2010) have been modified given the available radar measurements, vertical pointing Ka- and S-band radars, during the Midlatitude Continental Convective Clouds Experiment (MC3E) field campaign. For the estimation of RLWP, we will basically follow the idea described in Williams et al. (2016) to retrieve microphysical properties for raindrops, however instead of retrieving vertical air motion and rain DSDs (Williams et al., 2016), this study aims at retrieving RLWCs, and then integrating

RLWCs over the liquid layer to estimate RLWP. Overall, in this study, algorithms from three former publications are modified and combined to estimate the LWP in the stratiform precipitating systems.

The goals of this study are to retrieve the LWP, which includes both RLWP and CLWP retrievals using radars measurements, and tentatively answer two questions based on observations and retrievals in the stratiform precipitation systems during MC3E: (1) what is the occurrence of cloud below the melting base in the stratiform precipitation systems; (2) what are the values of simultaneous CLWP, RLWP and LWP, and how does CLWP or RLWP contribute to the LWP. Note that the CLWP and RLWP are constrained in a stratiform precipitation layer below the melting base and above the surface. The LWP estimations in this study are primarily aimed at stratiform precipitating events exhibiting melting-layer features from radar measurements with lower-to-moderate rain rates (RR < 10 mm hr^{-1}). The instruments and data used in this study are introduced in section 2. Section 3 describes the methods of retrieving LWP (both RLWP and CLWP). Section 4 illustrates two examples and followed by statistical results from more samples during MC3E. The last section gives the summary and conclusions. Acronyms and abbreviations are listed in Table 1.

2. Data

The MC3E field campaign, co-sponsored by the NASA Global Precipitation Measurement and the U.S. DOE ARM programs, was conducted at the ARM SGP (northern Oklahoma) during April-June 2011 to study convective clouds and improve model parametrization (Jensen et al., 2015). MC3E provided an opportunity to develop new retrieval methods to estimate cloud microphysics and precipitation properties in precipitation systems

(Giangrande et al., 2014; Williams, 2016; Tian et al., 2016; Tian et al, 2018). Several stratiform rain cases were observed by the VPRs during MC3E (as shown in Fig. 1). Distinct signatures of "bright banding" are detected from VPRs. To retrieve LWP associated with stratiform precipitation, this study mainly uses the observations from two co-located VPRs operating at 3-GHz and 35-GHz at DOE ARM SGP Climate Research Facility.

2.1 Vertical Pointing Radars

The 3-GHz (S-band) VPR was deployed by NOAA Earth System Research Laboratory for the six-weeks during the MC3E. The NOAA 3-GHz VPR is a vertical pointing radar with 2.6° beamwidth monitoring precipitation overhead. This 3-GHz profiler bridges the gap between cloud radars, which are used to provide the structure of nonprecipitating clouds but are severely attenuated by rainfall, and precipitation radars, which, although unattenuated by rainfall, generally lack the sensitivity to detect more detailed cloud structure. The 3-GHz VPR observes the raindrops within the Rayleigh scattering regime and its signal attenuation are negligible through the rain. The temporal resolution of the profiles of Doppler velocity spectra is 7 seconds and the vertical resolution is 60 meters. The 3-GHz VPR operated in two modes: a precipitation mode and a low-sensitivity mode. The precipitation mode observations are used in this study.

The Ka-band ARM zenith radar (KAZR) is also a vertical pointing radar, operating at 35 GHz permanently deployed by DOE ARM at the SGP site. The KAZR measurements include reflectivity, vertical velocity, and spectral width from near-ground to 20 km. The KAZR data used in this study are the KAZR Active Remote Sensing of Clouds (ARSCL) product produced by the ARM (www.arm.gov). The KAZR-ARSCL corrects for atmospheric gases attenuation and velocity aliasing. By selecting the mode with the highest signal-to-noise ratio at a given point, data from two simultaneous operating modes (general and cirrus mode) are combined for

Atmos. Meas. Tech. Discuss., https://doi.org/10.5194/amt-2018-388
Manuscript under review for journal Atmos. Meas. Tech.
Discussion started: 24 January 2019

Atmospheric Measurement Techniques Discussions

each profile to provide the "best estimates" of radar moments in the time-height fields. The vertical and temporal resolutions of KAZR-ARSCL product are 30 meters and 4 seconds, respectively. Since the 3-GHz and 35-GHz VPRs are independent radars with different dwell time and sample volumes (Williams et al., 2016), the radar observations are processed to 1-min temporal and 60-m vertical resolutions in this study.

2.2 Disdrometers

DOE ARM program maintains a suite of surface precipitation disdrometers. Measurements and estimations from the Distromet model RD-80 disdrometer and NASA two-dimensional video disdrometers (2DVD) deployed at the ARM SGP site are used in this study. The RD-80 disdrometer provides the most continuous raindrop size distribution (DSD) measurements at high spectral (20 size bins from 0.3 to 5.4 mm) and temporal resolutions (1 minute), and its minimal detectable precipitation amount is 0.006 mm hr^{-1}. From 2DVD, the rain DSDs are observed from 41 bins (0.1 - 10 mm), and its minimal detectable precipitation amount is 0.01 mm hr^{-1}. In addition to rain rate, the mean mass-weighted raindrop diameter (D_m) is also provided from 2DVD, which is used for evaluating retrieved D_m from radar measurements.

2.3 Ceilometer

A Vaisala laser ceilometer (CEIL) operates at the SGP Central Facility, sensing cloud presence up to a height of 7700m with 10-m vertical resolution. The laser ceilometer transmits near-infrared pulses of light, and the receiver detects the light scattered back by clouds and precipitation. It is designed to measure cloud-base height.

3. The Methodology of Liquid Water Path Estimation

As mentioned earlier, both RLWP and CLWP contribute to the LWP. With aid of the cloud base height detected by ceilometer, LWP is retrieved under two different situations: (I) the

Atmos. Meas. Tech. Discuss., https://doi.org/10.5194/amt-2018-388
Manuscript under review for journal Atmos. Meas. Tech.
Discussion started: 24 January 2019

Atmospheric Measurement Techniques Discussions
Open Access

cloud base is higher than the melting base and (II) the cloud base is lower than the melting base. For situation (I), there are almost no cloud droplets below melting base (CLWP = 0), and thus the LWP below the melting base is solely from raindrops. The LWP is calculated by integrating RLWCs over this layer. The RLWCs could be retrieved by analyzing the measured Doppler Velocity Differences ("*DVD Algorithm*") from two collocated VPRs. In situation (II), the small cloud droplets and large raindrops coexist below the melting base. Both raindrops and cloud particles contribute to LWP. RLWP will be still estimated using "*DVD Algorithm*". CLWP will be retrieved using an attenuation-based algorithm named as "*Attenuation Algorithm*". The algorithms for LWP estimation are summarized in a flowchart (Fig. 2).

3.1 Situation I (no cloud droplets exist below the melting base)

The algorithm from Williams et al. (2016) was developed based on an assumption that the 3-GHz VPR operates within the Rayleigh scattering regime for all raindrops, while the 35-GHz VPR operates within the Rayleigh scattering regime for small raindrops (diameters < ~1.3 mm) and non-Rayleigh scattering regime for larger raindrops (diameters ≥ ~1.3 mm). The different scattering regimes for the two operating frequencies result in different estimated radar moments. These estimated radar moments are in functions of rain microphysics. Thus, the rain microphysics could be retrieved with given measured radar moments. The details of this "*DVD Algorithm*" and uncertainty estimation are introduced in Appendix A.

3.2 Situation II (cloud particles and rain droplets coexist below the melting base)

In situation (II), substantial cloud particles exist below melting base, and both RLWP and CLWP retrievals are needed to estimate the LWP. The total two-way attenuation of 35-GHz VPR signals, A (in decibels, dB), in a layer between the melting base and the cloud base, mainly consists of rain attenuation, liquid clouds attenuation, and gaseous attenuation. The total attenuation (A) are expressed as:

$$A= 2\,C\,R_m\,\Delta H + 2\,B\,CLWP + G. \tag{1}$$

R_m is layer-mean rain rate, and ΔH (km) is the thickness of the layer (Matrosov, 2009). G is the two-way attenuation/absorption from atmospheric gases, which is relatively small, and the absorption by gases has been already corrected in the KAZR ARSCL dataset and is assumed to be zero in our retrieval.

C and B are the coefficients for rainfall and cloud liquid water attenuation.

$$B=0.0026\pi\lambda^{-1}\mathrm{Im}[-(m^2-1)(m^2+2)^{-1}], \tag{2}$$

where λ is the wavelength of Ka-band radar, and m is the complex refractive index of water. The unit of B is dB/g m^{-2}.

$$C = 0.27\,b, \tag{3}$$

where b is the correction factor considering raindrop fall velocities with changing air density.

$$b=(\rho_{am}/\rho_{a0})^{0.45}, \tag{4}$$

where ρ_{am} and ρ_{a0} are the mean air density in the rain layer and the density at normal atmospheric conditions.

Based on (1), CLWP can be written as:

$$CLWP = \frac{A-2\,C\,R_m\,\Delta H - G}{2\,B} \tag{5}$$

The attenuation (A) is estimated by comparing the drop in Ka-band reflectivity with the un-attenuated S-band reflectivity through the cloud. Assuming the changes in reflectivity with altitude due to changes in raindrop size distributions with altitude are similar for Ka- and S-band reflectivities, then the difference in reflectivities through the cloud is a proxy for attenuation. This can be expressed using

$$A \cong [Z_{Ka}(cloud\ base) - Z_{Ka}(melting\ base)] - [Z_S(cloud\ base) - Z_S(melting\ base)] \quad (6)$$

Notice that the absolute calibration of the radar was not important to the retrieval results since the retrieval of CLWP used S-Ka differential attenuation. This avoids the radar calibration (Tridon et al., 2015 and 2017), which is a serious issue limits the accuracy of radar retrievals.

The R_m is estimated as:

$$R_m = \frac{\sum_{CB}^{MB} RR(h) \times \Delta h}{\Delta H}, \quad (7)$$

where Δh equals 60 meters and MB and CB are the melting base and the cloud base. RRs in the layer between the melting base and the cloud base are calculated from the "*DVD algorithm*".

The uncertainties of retrieved CLWP are mainly due to the uncertainties of estimated R_m and observed total attenuation from VPRs. The value of B_k is on the order of 1 dB/kg m^{-2}. The uncertainty of retrieved CLWP would be ~ 0.25 kg m^{-2} with 0.5 dB uncertainty from measured radar reflectivity difference or ~ 0.5 kg m^{-2} for 1.0 mm hr^{-1} uncertainty from estimated layer-mean rain rate. Compared to the typical mean rain rate observed in the stratiform system (~ 2 - 4 mm hr^{-1}), 1.0 mm hr^{-1} represents a ~ 30% uncertainty. The uncertainty for CLWP retrievals is roughly estimated as ~ 0.56 kg m^{-2} (sqrt $(0.25^2+0.5^2)$) in this study. For reference, the expected uncertainty is reported as ~ 0.25 kg m^{-2} for typical rainfall rates (~ 3 - 4 mm hr^{-1}) in Matrosov (2009) retrieval method.

4. Retrieval Results and Discussions

4.1 Case Studies

Even though situation (I) is dominated (Fig. 1), especially in Case A, the ceilometer cloud base estimates can be lower than the melting base (Cases B to D). Two case studies (20

Atmos. Meas. Tech. Discuss., https://doi.org/10.5194/amt-2018-388
Manuscript under review for journal Atmos. Meas. Tech.
Discussion started: 24 January 2019

Atmospheric Measurement Techniques Discussions

May 2011 and 11 May 2011) are given as examples to demonstrate the estimation of LWP in stratiform precipitation system for two different situations.

4.1.1 Case A

On 20 May 2011, an upper level low-pressure system at central Great Basin moved into the central and northern Plains, while a surface low pressure at southeastern Colorado brought the warm and moist air from the southern Plains to a warm front over Kansas. and a dry line extended southward from the Texas-Oklahoma. With those favorable conditions, a strong north-south oriented squall line developed over Great Plains and propagated eastward. The convection along the leading edge of this intense squall line exited the ARM SGP network around 11 UTC 20 May leaving behind a large area of stratiform rain (Case A in Fig. 1). This stratiform system passed over the ARM SGP site and observed by two VPRs, and disdrometers as shown in Figures 1a-1c. It clearly shows the 3-GHz radar echo tops are much lower than those from the 35 GHz VPR. Even though there is attenuation at 35-GHz by the raindrops and melting hydrometeors, the 35-GHz radar can still detect more small ice particles at near the cloud top. The “bright band”, which occurs in a uniform stratiform rain region, is clearly seen from the 3-GHz VPR (a sudden increase and then decrease in radar reflectivity) but is not obvious from the 35-GHz VPR due to the non-Rayleigh scattering effects at 35 GHz (Sassen et al., 2005; Matrosov, 2008).

Figures 1a-1b clearly show that the ceilometer detected cloud base is in the middle of the melting layer, indicating almost no cloud particles below the melting layer and the LWP in the liquid layer equals to RLWP. The RLWP is retrieved using the “*DVD Algorithm*” introduced in section 3.1 and Appendix A. Figure 3 shows an example of the DVD retrieval algorithm at 13:40 UTC on May 20, 2011. Radar reflectivity from 3 GHz, Doppler velocities from 3 GHz and 35 GHz, and spectrum variance from 35 GHz are the inputs of DVD algorithm. The Doppler velocity differences (3 GHz – 35 GHz) from the surface to 4 km are also plotted in Fig. 3d. The melting base is defined as the height of maximum curvature in the radar reflectivity profile at 3 GHz (Fabry and Zawadzki, 1995), which is clearly seen at 2.5 km in Fig. 3. Below 2.5 km, the Doppler velocity differences between the two VPRs become relatively uniform, indicating that the process of melting snow/ice particles into raindrops is completed. Retrieved profiles of rain microphysical properties and their corresponding uncertainties (horizontal bars at different levels) in the rain layer (0 – 2.5 km) are shown in Figs 3f-3h. In general, the retrieved D_m values from the surface to 2.5 km are nearly a constant of ~2 mm (Fig. 3f), while the retrieved RLWC and rain rate values slightly decrease from 2.5 km to the surface. One of the highlights of this study is, in addition to the surface rain rate, which can usually be observed using surface disdrometers, the vertical profiles of rain microphysical properties are retrieved. These retrieved rain microphysical properties will shed light on the understanding of liquid cloud and rain microphysical processes (like condensation, evaporation, autoconversion and accretion etc.) in the models.

To evaluate the rain property retrievals, we compare the retrieved rain microphysical properties, the D_m, and rain rate at the surface, with the surface disdrometers measurements (Fig. 4). The D_m values range from 1.0 to 2.5 mm during a 3.5-hr period with nearly identical mean values of 1.79 mm and 1.81 mm from both retrievals and 2DVD measurements. There are large variations for rain rates, ranging from 0 to 8 mm hr^{-1}, with means of 3.19, 3.17 and 2.88 mm hr^{-1}, respectively, from 2DVD, RD-80 and radar retrieval. The mean rain rates from 2DVD and RD-80 measurements are almost the same although there are relatedly large differences during certain time periods, while the retrievals from this study, on average, underestimate the rain rate

Atmos. Meas. Tech. Discuss., https://doi.org/10.5194/amt-2018-388
Manuscript under review for journal Atmos. Meas. Tech.
Discussion started: 24 January 2019

by ~10% compared to the disdrometer measurements. More statistics (mean differences, their 95% confidence intervals of mean differences and root mean square errors) can be found in Table 2. Overall, the mean differences are within the retrieval uncertainties. The variation of RLWP (Fig. 4c) mimics the variation of retrieved rain rate in Fig. 4d. The mean value of RLWP is 0.56 kg m^{-2} for this case, which is also the LWP below the melting base.

4.1.2 Case B

On 11 May 2011, a surface cold front moved across the Oklahoma-Texas area and then convections were initiated. At 1600 UTC, a mesoscale convective system organized with a parallel stratiform precipitation region. Two-three hours later (~1830 UTC), the mesoscale convective system was transitioned to a trailing stratiform mode passed over the ARM SGP site. The large stratiform regions are observed by two VPRs and disdrometers as shown in Figs 1d-1f. Figures 1d-1f clearly show that the ceilometer detected cloud bases are lower than the melting bases occasionally. Under this situation, both RLWP and CLWP could contribute to the LWP below the melting base.

Firstly, the surface rain microphysics (D_m, RLWC, rain rate and RLWP) are retrieved using "*DVD Algorithm*". These rain property retrievals are compared with the surface disdrometers measurements (Fig. 5). The D_m values at the surface range from 0.8 to 2.2 mm during a 4.5-hr period with the mean values of 1.46 mm and 1.57 mm, respectively, from both retrievals and 2DVD measurements. The difference between the retrieval and 2DVD measurement may be due to different sampling volumes between radar and the surface disdrometer, as well as wind shear. To further investigate the difference, the measurements from five NASA 2DVDs located within 5 km away from VPRs are collected and processed. The almost same mean values and slight variation from 5 NASA 2DVDs measurements suggest that the difference between radar retrievals and the surface disdrometer measurements may be true, while averaging from more measurements can only smooth the variation.

The mean rain rate values from five NASA 2DVDs and the surface disdrometer are very comparable, with a mean difference of 0.3 mm hr^{-1}. The almost same mean values between the surface disdrometer and 5 NASA 2DVDs measurements suggest that the DVDs apart within 5 km can capture very similar rain properties during a longer time period, such as 4.5 hours in this case, although there are some large differences from their point-to-point measurements. The rain rates, in this case, vary quite large, ranging from 0 to 9 mm hr^{-1} with means of 1.81, 1.64 and 1.98 mm hr^{-1}, respectively from single 2DVD, RD-80, and our retrieval. It is found that, from both Case A and Case B, the mean value from RD-80 is smaller than that from 2DVD. This may be due to the different ranges of measurable drop sizes from two types of disdrometers (0.3 - 5.4 mm for RD 80, while 0.1 to 10 mm for 2DVD). More statistics can be also found in Table 2. Overall, the mean differences are still within the retrieval uncertainties for this case.

Secondly, the CLWP is retrieved using “Attenuation Algorithm” introduced in section 3.2. Figure 5c shows the time series of RLWP, CLWP and LWP retrievals. It is found that the CLWP values (when they exist) are usually larger than RLWP values in the same vertical column. When cloud droplets and raindrops coexist below the melting base, the mean values are 0.31 kg m^{-2} and 1.00 kg m^{-2} for RLWP and CLWP, and the corresponding LWP below the melting layer is 1.31 kg m^{-2}. While when only raindrops exist below the melting base, there is no CLWP (CLWP =0), and the RLWP and LWP are the same (with average of 0.33 kg m^{-2}). It is noticed that even though the occurrence of CLWP is low (12%) in this case, the value of CLWP can be very large when it exists, and it is about two times larger than the mean RLWP. The mean value of LWP is 0.45 kg m^{-2} for all the sample in Fig. 5c.

4.2 Statistical Results

Box and whisker plots of retrieved RLWP, CLWP and LWP for situations (I), (II) and all samples during MC3E are shown in Fig. 6. The horizontal orange and red dashed lines indicate the median and mean, boundaries of the box represent the first and third quartiles, and the whiskers are the 10^{th}- and 90^{th} -percentiles. During MC3E, a total of 14 hours of stratiform rain were observed by VPRs at the ARM SGP Climate Research Facility, in which 92% and 8% the samples are categorized into the situations (I) and (II), respectively. The mean RLWPs are 0.33 kg m^{-2} and 0.22 kg m^{-2} for the situations (I) and (II). There are a substantial amount of small cloud droplets sustaining in the rain layer and have not yet converted to larger raindrops, which may partially explain smaller RLWP in the situation (II). The mean value of surface rain rate is 1.78 mm hr^{-1} when cloud droplets exist, which is also smaller than the mean value (2.06 mm hr^{-1}) in the rain-only situation. The mean CLWP in the situation (II) is as large as ~0.87 kg m^{-2} even though their occurrence is very low (8%), which is much larger than mean RLWP in the liquid layer. The ratio of RLWP and CLWP ranges from 4:1 to 2:1 for precipitating shallow marine clouds reported at Lebsock et al. (2011), while our results from MC3E do not seem to have a clear linear relationship between CLWP and RLWP (figure is not shown). The LWP from the situation (II) is much larger than the mean LWP from the situation (I), which is primarily contributed by cloud droplets. The overall mean LWP for stratiform rain during MC3E is 0.39 kg m^{-2}.

We also processed the ARM MWR retrieved LWPs during MC3E and compared with our retrievals as illustrated in Fig. 7. Statistical results of the retrieved LWPs from this study and MWR are averaged for each measured rain rate bins (bin size = 0.25 mm hr^{-1}). When the rain rate is greater than ~ 6mm hr^{-1}, there are no MWR LWP retrievals. Fig. 7b shows that the MWR retrieved LWPs, as expected, monotonically increase with rain rate, which is possible due to the

Atmos. Meas. Tech. Discuss., https://doi.org/10.5194/amt-2018-388
Manuscript under review for journal Atmos. Meas. Tech.
Discussion started: 24 January 2019

Atmospheric Measurement Techniques Discussions

"wet radome" effect (Cadeddu et al., 2017). "Wet radome" is a particularly complicated situation because the standing water often looks physically like a layer and less like a collection of drops, making the MWR overestimate LWPs (personal communication with Dave Turner, 2018), and so far, no effective method was found to solve this problem (Cadeddu et al., 2017).

In addition to the issue from standing water on the radome, the scattering effects due to raindrops also affect MWR retrievals. Two general retrieval methods are commonly used to retrieve LWP from the observed brightness temperatures: statistical methods (Liljegren et al., 2001) and physical retrievals (Turner et al, 2007). No matter which retrieval is used, the radiative transfer code usually only models the absorptions from atmospheric gases and cloud liquid water. The scattering effect is not taken into consideration during the retrieval, that is, it is under the assumption that the brightness temperature is primarily due to the emission of cloud droplets in the MWR retrieval. Even small drizzle particles still have a scattering effect, which could contribute higher brightness temperature measured by MWR and result in larger retrieved LWPs than the "true" LWPs. Therefore, the MWR retrieved LWPs are most likely overestimated for precipitating clouds.

In this study, we mainly focus on the stratiform rain systems with mean rain rates of 2-4 mm hr^{-1}. The scattering effect for large raindrops is more significant than drizzles. Sheppard (1996) examined the effect of raindrops on MWR brightness temperature measurements at 31 GHz and found that cloud absorption coefficient is only ~2/3 of rain absorption coefficient, however, the scattering effect of raindrops is not insignificant where its scattering coefficient is about half of cloud absorption coefficient. Thus, MWR measured brightness temperatures for precipitating clouds would be higher, due to the scattering by raindrops, than those for non-precipitating clouds, and then result in higher LWPs than the 'true" LWPs. The differences of

LWPs from MWR and this study are shown in Fig. 7c. The LWP differences increase almost linearly with increased rain rate. The differences could be due to (1) MWR retrieved LWP represents the whole vertical column (RWLP and CLWP below melting layer, large water coated ice particles in the melting layer and supercooled LWCs above the melting layer), while our retrieval only represent the LWP below the melting base; (2) existing uncertainty in retrieved LWP from this study (~0.6 kg m^{-2} when includeing CLWP estimates).

5. Summary and Conclusions

LWP is a critical parameter for studying clouds, precipitation, and their life cycles. LWP can be retrieved from microwave radiometer measured brightness temperatures during cloudy and light precipitation conditions. However, MWR-retrieved LWPs are questionable under moderate and heavy precipitation conditions due to the "wet radome" and non-Rayleigh scattering effects caused by large raindrops. LWPs below the melting base in stratiform precipitation systems are estimated, which include both RLWP and CLWP. The measurements used in this study are mainly from two VPRs, 35-GHz from ARM and 3-GHz from NOAA during the MC3E field campaign.

In this study, the microphysical properties of raindrops, such as D_m, RLWC (and RLWP), and RR, are estimated following the method described in Williams et al. (2016) using measurements from co-located Ka- and S-band radars VPRs. The retrieved rain microphysical properties are validated by the surface disdrometer measurements. Instead of retrieving vertical air motion and rain DSDs (Williams et al., 2016), this study aims at retrieving RLWCs and then integrating RLWCs over the liquid layer to estimate RLWP. The CLWP is retrieved based on

Atmos. Meas. Tech. Discuss., https://doi.org/10.5194/amt-2018-388
Manuscript under review for journal Atmos. Meas. Tech.
Discussion started: 24 January 2019

the modifications of the methods in Matrosov (2009 and 2010) with available radar measurements, vertical pointing Ka- and S-band VPRs, during the MC3E field campaign.

The applicability of retrieval methods is illustrated for two stratiform precipitation cases (20 May 2011 and 11 May 2011) observed during MC3E. Statistical results from a total of 14 hours samples during MC3E show that the occurrence of cloud droplets below the melting base is low (8%), while the CLWP value can be up to 0.87 kg m^{-2}, which is much larger than the RLWP (0.22 kg m^{-2}). When only raindrops exist below the melting base, the averaged RLWP value is 0.33 kg m^{-2}, which is much larger than the mean RLWP in the cloud droplets and raindrops coexisted situation.

Reliable retrievals of RLWC and RLWP are critical for model evaluation and improvement, as RLWC (rain mixing ratio) is an important prognostic variable in weather and climate models. Furthermore, the retrievals in the whole rain layer would be useful to understand the microphysical processes (i.e., condensation, evaporation, autoconversion, and accretion etc.) and have great potential to improve model parametrizations in the future. Overall, the LWP (CLWP and RLWP) retrievals derived in this study can be used to evaluate the models that separately predict cloud and precipitation separately, and contribute comprehensive information to study cloud-to-precipitation transitions.

Appendix A: Doppler Velocity Differences Algorithm ("*DVD Algorithm*")

Retrieving RLWC and other rain microphysical properties (i.e., drop size and rain rate) is based on the mathematics of DSD radar reflectivity-weighted velocity spectral density S_{DSD}^{λ} [(mm^6 m^{-3}) (m s^{-1})$^{-1}$], which is a product of radar raindrop backscattering cross section σ_b^{λ}(D) (mm^2) and DSD number concentration N_{DSD}(D) (mm^{-1} m^{-3}):

Atmos. Meas. Tech. Discuss., https://doi.org/10.5194/amt-2018-388
Manuscript under review for journal Atmos. Meas. Tech.
Discussion started: 24 January 2019

$$S_{DSD}^{\lambda}(v_z) = [\frac{\lambda^4}{\pi^5|K_w|^2}\sigma_b^{\lambda}]N_{DSD}(D)\frac{dD}{dv_z}\,. \quad \text{(A1)}$$

The $\frac{dD}{dv_z}$ [mm (m s^{-1})$^{-1}$] is used as a coordinate transformation from diameter to velocity, where v_z (m s^{-1}) is the raindrop terminal velocity of diameter D (mm) at altitude z. λ is the wavelength of radar. $|K_w|^2$ equals 0.93 and it is the dielectric factor.

The N_{DSD}(D) can be expressed as a normalized gamma shape distribution with a three parameters (Leinonen et al., 2012):

$$N_{DSD}(D; N_w, D_m, \mu) = N_w f(D;\ D_m, \mu), \quad \text{(A2)}$$

where

$$f(D;\ D_m, \mu) = \frac{6}{4^4}\frac{(\mu+4)^{(\mu+4)}}{\Gamma(\mu+4)}(\frac{D}{D_m})^{\mu}\exp\left[-(\mu+4)\frac{D}{D_m}\right]. \quad \text{(A3)}$$

N_w is the scaling parameter, μ is a shape parameter, $\Gamma(x)$ is the Euler gamma function, and D_m is a mean mass-weighted raindrop diameter estimated from the ratio of the fourth to third DSD moments:

$$D_m = \frac{M_4}{M_3} = \frac{\int_{D_{min}}^{D_{max}} N_{DSD}(D)D^4 dD}{\int_{D_{min}}^{D_{max}} N_{DSD}(D)D^3 dD}\,. \quad \text{(A4)}$$

where D_{min} and D_{max} represent the minimum and maximum diameters in the distribution, respectively.

The intrinsic (non-attenuation) reflectivity factor and the mean velocity and the spectrum variance are the zeroth, first, and second reflectivity-weighted velocity spectrum moments :

$$Z_{DSD}^{\lambda} = \sum_{v_{min}}^{v_{max}} S_{DSD}^{\lambda}(v_i)\Delta v \quad \text{(A5)}$$

$$v_{DSD}^{\lambda} = \frac{\sum_{v_{min}}^{v_{max}} S_{DSD}^{\lambda}(v_i)\, v_i\, \Delta v}{Z_{DSD}^{\lambda}} \quad \text{(A6)}$$

$$SV_{DSD}^{\lambda} = \frac{\sum_{v_{min}}^{v_{max}} (v_i - v_{DSD}^{\lambda})^2 S_{DSD}^{\lambda}(v_i)\, \Delta v}{Z_{DSD}^{\lambda}}. \quad \text{(A7)}$$

Atmos. Meas. Tech. Discuss., https://doi.org/10.5194/amt-2018-388
Manuscript under review for journal Atmos. Meas. Tech.
Discussion started: 24 January 2019

Atmospheric Measurement Techniques
Discussions

where v_i is the discrete velocities and Δv is velocity resolution in the integration. The Doppler Velocity Difference (DVD) is defined as

$$\mathrm{DVD} = \mathrm{v}_{\mathrm{DSD}}^{3\ \mathrm{GHz}} - \mathrm{v}_{\mathrm{DSD}}^{35\ \mathrm{GHz}}. \quad \text{(A8)}$$

Note that both DVD and SV are dependent on DSD parameters (D_m and μ) only.

The RLWC and rain rate (RR) can also be described using the DSD:

$$\mathrm{RLWC}(\mathrm{g\ m^{-3}}) = \frac{\pi}{6}10^{-3}\sum_{\mathrm{D_{min}}}^{\mathrm{D_{max}}} \mathrm{N_{DSD}}(\mathrm{D}, \mathrm{N_w}, \mathrm{D_m}, \mu)\mathrm{D_i^3}\Delta\mathrm{D} \quad \text{(A9)}$$

$$\mathrm{RR}(\mathrm{mm\ hr^{-1}}) = \frac{6\pi}{10^4}\sum_{\mathrm{D_{min}}}^{\mathrm{D_{max}}} \mathrm{N_{DSD}}(\mathrm{D}, \mathrm{N_w}, \mathrm{D_m}, \mu)\mathrm{D_i^3}\mathrm{v_z}(\mathrm{D_i})\Delta\mathrm{D}. \quad \text{(A10)}$$

In addition, there are two newly defined radar-related parameters ($Z_{3GHZ}LWC$ and $Z_{3GHZ}RR$), which are also dependent on D_m and μ only:

$$Z_{3GHZ}LWC=10\ \log_{10}(Z_{DSD}^{3GHz}/RLWC) \quad \text{(A11)}$$

$$Z_{3GHZ}RR=10\ \log_{10}(Z_{DSD}^{3GHz}/RR) \quad \text{(A12)}$$

In this study, four variables, DVD, SV at 35 GHz (SV_{35GHz}), $Z_{3GHZ}LWC$ and $Z_{3GHZ}RR$, are pre-calculated using different groups of D_m and μ values, and then these values are stored in look-up tables (LUTs). Raindrop backscattering cross sections are calculated using the T-matrix with different temperatures and oblate raindrop axis ratios (Leinonen, 2014). LUT examples are illustrated in Fig. A as functions of DVD and SV_{35GHz}. If we assume that the observed radar Doppler velocity difference and spectrum variance from the 35-GHz radar is equal to the DSD velocity difference and variance (DVD and SV_{35GHz}), the measured Doppler velocity difference and spectrum variance at 35-GHz can determine a solution for D_m from the LUT (Fig. A(a)). Similarly, a value of $Z_{3GHZ}LWC$ (or $Z_{3GHZ}RR$) can be found with measured DVD and SV_{35GHz} using the LUT in Fig. A(b) (or Fig. A(c)). Then RLWC (or RR) can be estimated using (A11) (or (A12)) with measured reflectivity at 3-GHz (Z_{3GHZ}).

Atmos. Meas. Tech. Discuss., https://doi.org/10.5194/amt-2018-388
Manuscript under review for journal Atmos. Meas. Tech.
Discussion started: 24 January 2019

Atmospheric Measurement Techniques Discussions

The observed radar Doppler velocity difference can be assumed to be equal to the DSD velocity difference for two reasons: (1) even though the radar observed Doppler velocity spectrum can be broaden by the air motion, this spectrum broadening variance is small (within 2%) relative to the DSD velocity spectrum because of the narrow beamwidth (0.2°) of KAZR and (2) spectrum broadening is symmetric, which does not affect the first spectrum moment and the DSD mean Doppler velocity only shifts due to the air motion. Therefore, the measured differences of Doppler velocity between the 3-GHz and 35- GHz radars vertical pointing observations are independent of air motion and can be assumed to be the same as DVD from (A8). The validity of such an assumption is fully discussed in Williams et al. (2016).

The variabilities of 3-GHz and 35-GHz VPR observations within each 1-minute/60-meter bin are regarded as the measurement uncertainties and will be propagated through the retrieval to produce retrieval uncertainties. The retrieval uncertainties are estimated follow two steps: (1) construct a distribution of input radar measurements. For example, the temporal resolution for 3-GHz VPR is seven seconds, thus there are about nine radar reflectivities observed for one minute. A normal distribution is generated first using the mean and standard deviations of these nine observed radar reflectivities for this 1-min/60-m resolution/bin. (2) repeat the DVD retrievals using samplings from distributions of all input measurements. We randomly select 100 groups of members from those (DVD, SV_{35GHz}, Z_{3GHZ}) normal distributions to form 100 realizations, and then produce 100 separate output estimates. The mean and standard deviation of the 100 solutions are regarded as the final retrieval and the retrieval uncertainty.

It is noted that the uncertainty here only considers estimates of instrument noise, not the uncertainties associated with assumptions used in the retrieval. For example, the gamma size distribution used in (A2) is an approximation which may introduce error into the retrieval.

However, it is very difficult to quantify this type of retrieval uncertainty. In this study, we further compared our retrievals with independent surface disdrometers measurements to estimate the uncertainties of retrievals. Also, when both radars are observing at Rayleigh scattering for small raindrops, the reflectivity-weighted radial velocities for these particles should be the same. In order to have a difference in radial velocity during the retrieval, large droplets must exist. The maximum diameters in drop size distribution measured from disdrometer for all the stratiform cases during MC3E are investigated. It is found that the occurrence of small-droplets-only (maximum diameter <1.3 mm) is very low (less than 3%). Thus, it will not have a significant impact on the retrieval results. Notice that this algorithm is not suitable for strong convective rain due to the wind shear and strong turbulence as well as severe attenuation and extinction of the Ka-band radar signal.

Acknowledgments: J. Tian and X. Dong are supported by DOE CMDV project under grant DE-SC0017015 at the University of Arizona, and B. Xi is supported by NASA CERES project under grant NNX17AC52G at the University of Arizona. C. R. Williams is supported by DOE ASR project under grant DE-SC0014294. Special thanks to Dr. Sergey Matrosov from NOAA Earth System Research Laboratory (ESRL) for his suggestions. Special thanks to Michael Jensen, PI of MC3E. Aircraft in situ measurements are processed using data from https://ghrc.nsstc.nasa.gov/pub/fieldCampaigns/gpmValidation/mc3e/, can also be obtained from Xiquan Dong (xdong@email.arizona.edu). NOAA vertical profile radar datasets are publically available in the DOE archives (http://iop.archive.arm.gov/arm-iop/2011/sgp/mc3e/williams-s_band/).

Atmos. Meas. Tech. Discuss., https://doi.org/10.5194/amt-2018-388
Manuscript under review for journal Atmos. Meas. Tech.
Discussion started: 24 January 2019

Atmospheric Measurement Techniques Discussions

References

Ackerman, T. P., and Stokes, G. M: The Atmospheric Radiation Measurement Program. Phys. Today, 56,38–44, doi:10.1063/1.1554135, 2003

Battaglia, A., Saavedra, P., T. Rose, and Simmer, C.: Characterization of precipitating clouds by ground-based measurements with the triple-frequency polarized microwave radiometer ADMIRARI, J. Appl. Meteorol., 49(3), 394–414, 2009

Cadeddu, M. P., Liljegren, J. C., and Turner, D. D.: The Atmospheric radiation measurement (ARM) program network of microwave radiometers: instrumentation, data, and retrievals, Atmos. Meas. Tech., 6, 2359-2372, https://doi.org/10.5194/amt-6-2359-2013, 2013

Cadeddu, M. P., Marchand, R., Orlandi, E., Turner, D. D. and Mech, M. (2017). Microwave Passive Ground-Based Retrievals of Cloud and Rain Liquid Water Path in Drizzling Clouds: Challenges and Possibilities, IEEE Transactions on Geoscience and Remote Sensing, vol. 55, no. 11, pp. 6468-6481, doi: 10.1109/TGRS.2017.2728699

Crewell, S., and Löhnert, U. (2003). Accuracy of cloud liquid water path from ground-based microwave radiometry 2. Sensor accuracy and synergy, Radio Sci., 38, 8042, doi:10.1029/2002RS002634, 3.

Dubrovina, L. S.: Cloudness and precipitation according to the data of airplane soundings, Gidrometeoizdat, Leningrad (in Russian), 218 pp,1982

Ellis, S. M., and Vivekanandan, J.: Liquid water content estimates using simultaneous S and K_a band radar measurements, Radio Sci., 46, RS2021, doi:10.1029/2010RS004361, 2011

Fabry, F. and Zawadzki, I.: Long-Term Radar Observations of the Melting Layer of Precipitation and Their Interpretation. J. Atmos. Sci., 52, 838–851, https://doi.org/10.1175/1520-0469(1995)052<0838:LTROOT>2.0.CO;2, 1995

Fan, J., Liu, Y.-C., Xu, K.-M., North, K., Collis, S., Dong, X, and Ghan, S. J.: Improving representation of convective transport for scale-aware parameterization:1. Convection and cloud properties simulated with spectral bin and bulk microphysics, Journal of Geophysical Research: Atmosphere, 120, 3485–3509, https://doi.org/10.1002/2014JD022142, 2015

Feng, Z., Dong, X. Q., Xi, B. K., Schumacher, C., Minnis, P., and Khaiyer, M.: Top-of-atmosphere radiation budget of convective core/stratiform rain and anvil clouds from deep convective systems. Journal of Geophysical Research, 116, D23202. https://doi.org/10.1029/2011JD016451, 2011

Feng, Z., Leung, L. R., Houze, R. A., Jr., Hagos, S., Hardin, J., Yang, Q., Han, B. and Fan, J.: Structure and evolution of mesoscale convective systems: Sensitivity to cloud microphysics in convection-permitting simulations over the United States. Journal of Advances in Modeling Earth Systems, 10, 1470–1494. https://doi.org/10.1029/2018MS001305, 2018

Giangrande, S. E., Collis, S., Theisen, A. K., and Tokay, A.: Precipitation estimation from the ARM distributed radar network during the MC3E campaign, J. Appl. Meteorol. Climatol., doi:10.1175/JAMC-D-13-0321.1, 2014

Jensen, M.P., Petersen, W. A., Bansemer, A., Bharadwaj, N., Carey, L. D., Cecil, D. J, and Zipser, E. J.: The Midlatitude Continental Convective Clouds Experiment (MC3E), Bulletin of the American Meteorological Society. 151221073208006. https://doi.org/10.1175/BAMS-D-14-00228.1, 2015

Leinonen, J., Moisseev, D., M. Leskinen, M., and W.A. Petersen, W.A.: A Climatology of Disdrometer Measurements of Rainfall in Finland over Five Years with Implications for

Global Radar Observations. J. Appl. Meteor. Climatol., 51, 392–404, https://doi.org/10.1175/JAMC-D-11-056.1, 2012

Leinonen, J.: High-level interface to T-matrix scattering calculations: architecture, capabilities and limitations, Opt. Express, vol. 22, issue 2, 1655-1660 doi: 10.1364/OE.22.001655, 2014

Liljegren, J. C., Clothiaux, E. E., Mace, G. G., Kato, S., and Dong, X.: A new retrieval for cloud liquid water path using a ground-based microwave radiometer and measurements of cloud temperature, J. Geophys. Res., 106(D13), 14485–14500, doi:10.1029/2000JD900817, 2001

Lebsock, M.D., L'Ecuyer, T.S. and Stephens, G.L.: Detecting the Ratio of Rain and Cloud Water in Low-Latitude Shallow Marine Clouds. J. Appl. Meteor. Climatol., 50, 419–432, https://doi.org/10.1175/2010JAMC2494.1, 2011

Matrosov, S. Y.: Assessment of radar signal attenuation caused by the melting hydrometeor layer. IEEE Trans. Geo Sci. Remote Sens.,46,1039–1047 doi: 10.1109/TGRS.2008.915757, 2008

Matrosov, S. Y.: A method to estimate vertically integrated amounts of cloud ice and liquid and mean rain rate in stratiform precipitation from radar and auxiliary data, J. Appl. Meteorol., 48, 1398–1410, doi:10.1175/2009JAMC2196.1, 2009

Matrosov, S. Y.: Synergetic use of millimeter- and centimeter-wavelength radars for retrievals of cloud and rainfall parameters, Atmos. Chem. Phys., 10, 3321-3331, https://doi.org/10.5194/acp-10-3321-2010, 2010

Mazin, I. P. (Ed.): Clouds and the Cloudy Atmosphere. Gidrometeoizdat, Leningrad, 648 pp, 1989.

Saavedra, P., Battaglia, A., and Simmer, C.: Partitioning of cloud water and rainwater content by ground-based observations with the Advanced Microwave Radiometer for Rain Identification (ADMIRARI) in synergy with a micro rain radar, J. Geophys. Res., 117, D05203, doi:10.1029/2011JD016579, 2012

Sassen, K., Campbell, J. R., Zhu, J., Kollias, P., Shupe, M., and Williams, C.: Lidar and Triple-Wavelength Doppler Radar Measurements of the Melting Layer: A Revised Model for Dark- and Brightband Phenomena. J. Appl. Meteor., 44, 301–312, https://doi.org/10.1175/JAM-2197.1, 2005

Sheppard, B.E.: Effect of Rain on Ground-Based Microwave Radiometric Measurements in the 20–90-GHz Range. *J. Atmos. Oceanic Technol.,* 13, 1139–1151, https://doi.org/10.1175/1520-0426(1996)013<1139:EOROGB>2.0.CO;2, 1996

Tian, J., Dong, X., Xi, B., Wang, J., Homeyer, C. R., McFarquhar, G. M., and Fan J.: Retrievals of ice cloud microphysical properties of deep convective systems using radar measurements, Journal of Geophysical Research: Atmosphere., 121,10 ,820–10,839, https://doi.org/10.1002/2015JD024686, 2016

Tian, J., Dong, X., Xi, B., Minnis, P., Smith, W. L., Jr, Sun-Mack, S., … Wang, J.: Comparisons of ice water path in deep convective systems among ground-based, GOES, and CERES-MODIS retrievals. Journal of Geophysical Research: Atmospheres, 123, 1708–1723. https://doi.org/10.1002/2017JD027498, 2018

Tridon, F., and Battaglia, A.: Dual-frequency radar Doppler spectral retrieval of rain drop size distributions and entangled dynamics variables, J. Geophys. Res. Atmos., 120, 5585–5601, doi:10.1002/2014JD023023, 2015

Atmos. Meas. Tech. Discuss., https://doi.org/10.5194/amt-2018-388
Manuscript under review for journal Atmos. Meas. Tech.
Discussion started: 24 January 2019

Atmospheric Measurement Techniques
Open Access
Discussions

Tridon, F., Battaglia, A., and Kollias, P.: Disentangling Mie and attenuation effects in rain using a Ka-W dual-wavelength Doppler spectral ratio technique, Geophys. Res. Lett., 40, 5548 5552, doi:10.1002/2013GL057454, 2013

Tridon, F., Battaglia, A., Luke, E., and Kollias, P.: Rain retrieval from dual-frequency radar Doppler spectra: validation and potential for a 25 midlatitude precipitating case-study, Quarterly Journal of the Royal Meteorological Society, 143, 1364–1380, 2017.

Turner, D. D., Clough, S. A., Liljegren, J. C., Clothiaux, E. E., Cady-Pereira, K. E., and Gaustad, K. L.: Retrieving liquid water path and precipitable water vapor from the Atmospheric Radiation Measurement (ARM) microwave radiometers. IEEE Trans. Geosci. Remote Sens., 45, 3680–3690, 2007

Wentz, F.J. and Spencer, R.W.: SSM/I Rain Retrievals within a Unified All-Weather Ocean Algorithm. J. Atmos. Sci., 55, 1613–1627, https://doi.org/10.1175/1520-0469(1998)055<1613:SIRRWA>2.0.CO;2, 1998

Williams, C. R.: Reflectivity and liquid water content vertical decomposition diagrams to diagnose vertical evolution of raindrop size distributions, J. Atmos. Oceanic Technol., doi:10.1175/JTECH-D-15-0208.1, 2016

Williams, C. R., Beauchamp, R. M., and Chandrasekar, V.: Vertical air motions and raindrop size distributions estimated from mean Doppler velocity difference from 3- and 35-GHz vertically pointing radars. IEEE Transactions on Geoscience and Remote Sensing, 54, 6048–6060, https://doi.org/10.1109/ TGRS.2016.2580526, 2016

Xu, W.: Precipitation and convective characteristics of summer deep convection over east Asia observed by TRMM, Monthly Weather Review., 141, 1577-1592. https://doi.org/10.1175/MWR-D-12-001

Atmos. Meas. Tech. Discuss., https://doi.org/10.5194/amt-2018-388
Manuscript under review for journal Atmos. Meas. Tech.
Discussion started: 24 January 2019

Table 1. Acronyms and Abbreviations Used in This Study

Acronyms and Abbreviations	Full Name
2DVD	Two-dimensional video disdrometer
A	Total two-way attenuation of 35-GHz VPR signals
ARSCL	Active remote sensing of clouds
ARM	Atmospheric Radiation Measurement
B	coefficients for cloud water attenuation
C	coefficients for rainfall attenuation
CLWP	Cloud liquid water path
D	Raindrop diameter
D_m	Mean mass-weighted raindrop diameter
D_{max}	Maximum diameters in the size distribution
D_{min}	Minimum diameters in the size distribution
DOE	Department of Energy
DSD	Drop size distribution
DVD	Doppler velocity difference
G	Two-way gaseous absorption
IWC	Ice water content
KAZR	Ka-band ARM zenith radar
LUT	Looking up table
LWP	Liquid water path
MB	Base of melting layer
MC3E	Mid-latitude continental convective clouds experiment
MMCR	Millimeter-wavelength cloud radar
MWR	Microwave radiometer
N_{DSD}	Number concentration
N_0	Intercept of ice particle size distribution
NOAA	National Oceanic and Atmospheric Administration
N_w	Scaling parameter in the drop size distribution
RLWP	Rain liquid water path
R_m	Layer-mean rain rate
RR	Rain rate

Atmos. Meas. Tech. Discuss., https://doi.org/10.5194/amt-2018-388
Manuscript under review for journal Atmos. Meas. Tech.
Discussion started: 24 January 2019

$\mathbf{S_{DSD}^{\lambda}}$	Radar reflectivity-weighted velocity spectral density
$\mathbf{v_{DSD}^{\lambda}}$	First reflectivity-weighted velocity spectrum moments represent the mean velocity
Vz	Raindrop terminal velocity
$\mathbf{Z_{DSD}^{\lambda}}$	Zeroth reflectivity-weighted velocity spectrum moments represent the intrinsic (non-attenuation) reflectivity factor
$\mathbf{\Gamma(x)}$	Euler gamma function
λ	Radar wavelength
$\mathbf{\sigma_b^{\lambda}}$	Raindrop backscattering cross section
μ	Shape parameter

Atmos. Meas. Tech. Discuss., https://doi.org/10.5194/amt-2018-388
Manuscript under review for journal Atmos. Meas. Tech.
Discussion started: 24 January 2019

Table 2. Statistics (mean differences, 95% confidence interval of mean differences, RMSEs) of D_m, RR between this study (RET) and disdrometers (2DVD, RD-80) for Case A and Case B

	Mean Differences (95% confidence interval)	RMSE
Case A: D_m (RET, 2DVD) (mm)	-0.02 (-0.05, 0.01)	0.24
Case A: RR (RET, RD-80) (mm hr^{-1})	-0.29 (-0.40, -0.19)	0.98
Case A: RR (RET, 2DVD) (mm hr^{-1})	-0.31(-0.48, -0.15)	1.45
Case B: D_m (RET, 2DVD) (mm)	-0.11 (-0.14, -0.07)	0.29
Case B: D_m (RET, 2DVD-all) (mm)	-0.09 (-0.13, -0.05)	0.34
Case B: RR (RET, RD-80) (mm hr^{-1})	0.34 (0.16,0.53)	1.63
Case B: RR (RET, 2DVD) (mm hr^{-1})	0.17(-0.01,0.36)	1.61
Case B: RR (RET, 2DVD-all) (mm hr^{-1})	0.14 (-0.08,0.36)	1.89

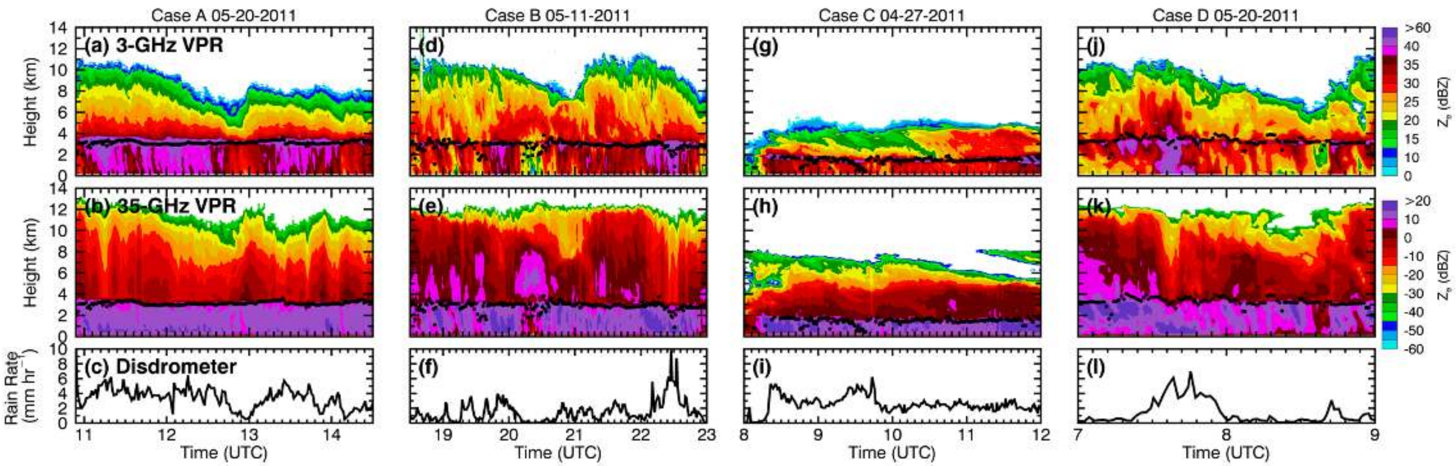

Figure 1. Time series of (a) radar reflectivity (Z_e) from NOAA 3-GHz vertical pointing radar (VPR), (b) radar reflectivity from ARM 35-GHz VPR, and (c) rain rates from RD-80 surface disdrometer measurement for Case A (20 May 2011, 11:00 – 15 :30 UTC); (d)-(f) for Case B (11 May 201, 18:30 – 23 :00 UTC); (g)-(i) for Case C (27 April 2011, 8:00 – 12 :00 UTC); (j)-(l) for Case D (20 May 2011, 7:00 – 9 :00 UTC). Ceilometer cloud base height estimates are shown with black dots at 1-minute resolution. Note that the ranges of radar dBZ values are different in 3-GHz and 35-GHz radars.

Atmos. Meas. Tech. Discuss., https://doi.org/10.5194/amt-2018-388
Manuscript under review for journal Atmos. Meas. Tech.
Discussion started: 24 January 2019

Atmospheric Measurement Techniques
Discussions

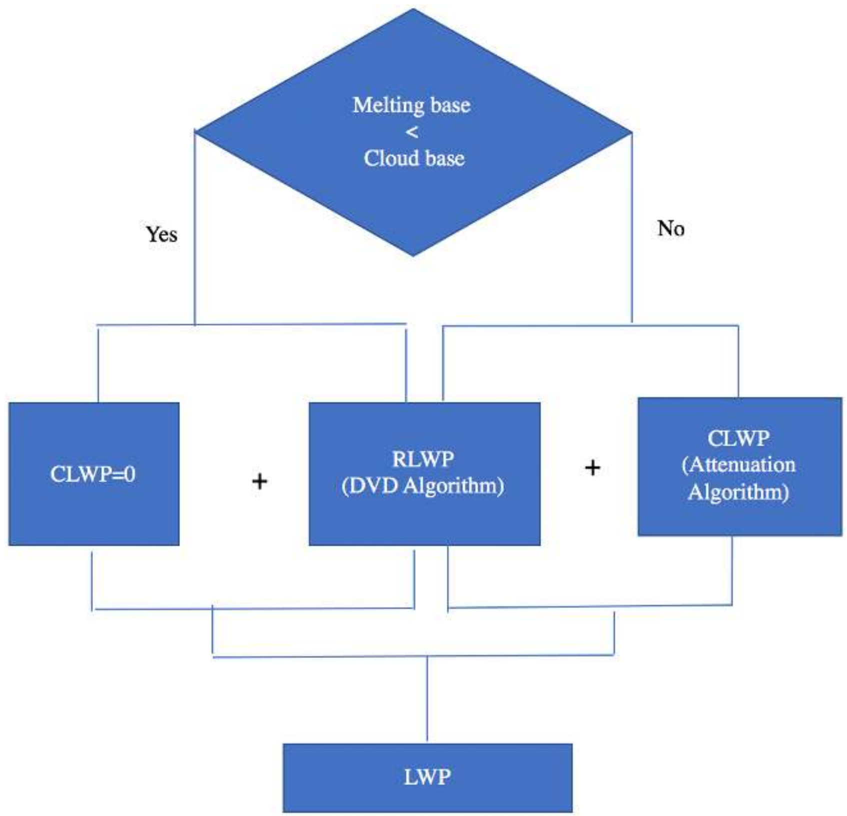

Figure 2. Algorithm flowchart to retrieve liquid water path (LWP) below melting base.

Atmos. Meas. Tech. Discuss., https://doi.org/10.5194/amt-2018-388
Manuscript under review for journal Atmos. Meas. Tech.
Discussion started: 24 January 2019

Atmospheric Measurement Techniques
Discussions

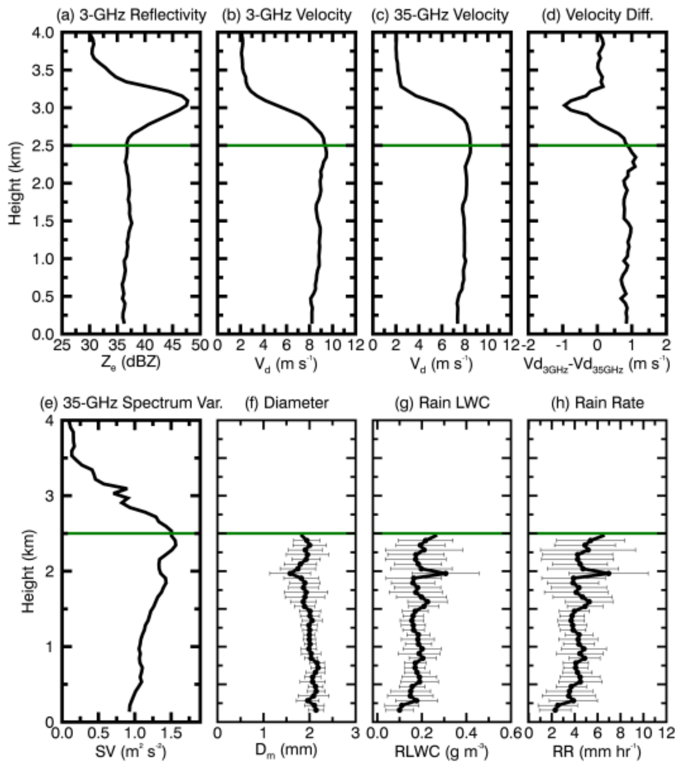

Figure 3. An example of illustrating the Doppler Velocity Differences (DVD) retrieval algorithm at 13:40 UTC on May 20, 2011. The inputs of the DVD retrieval algorithm are: (a) 3-GHz vertical pointing radar reflectivity factor (Z_e), (b) 3-GHz radar Doppler velocities (V_d), (c) 35-GHz radar Doppler velocities (V_d), and (e) 35-GHz radar spectrum variances (SV). The Doppler velocity difference between 3-GHz and 35 GHz is shown in (d). The outputs of the DVD retrieval algorithm are: (f) mass-weighted mean diameter D_m, (g) rain liquid water content (RLWC), and (h) rain rate (RR). Retrieval uncertainties are shown as horizontal thin black lines.

Atmos. Meas. Tech. Discuss., https://doi.org/10.5194/amt-2018-388
Manuscript under review for journal Atmos. Meas. Tech.
Discussion started: 24 January 2019

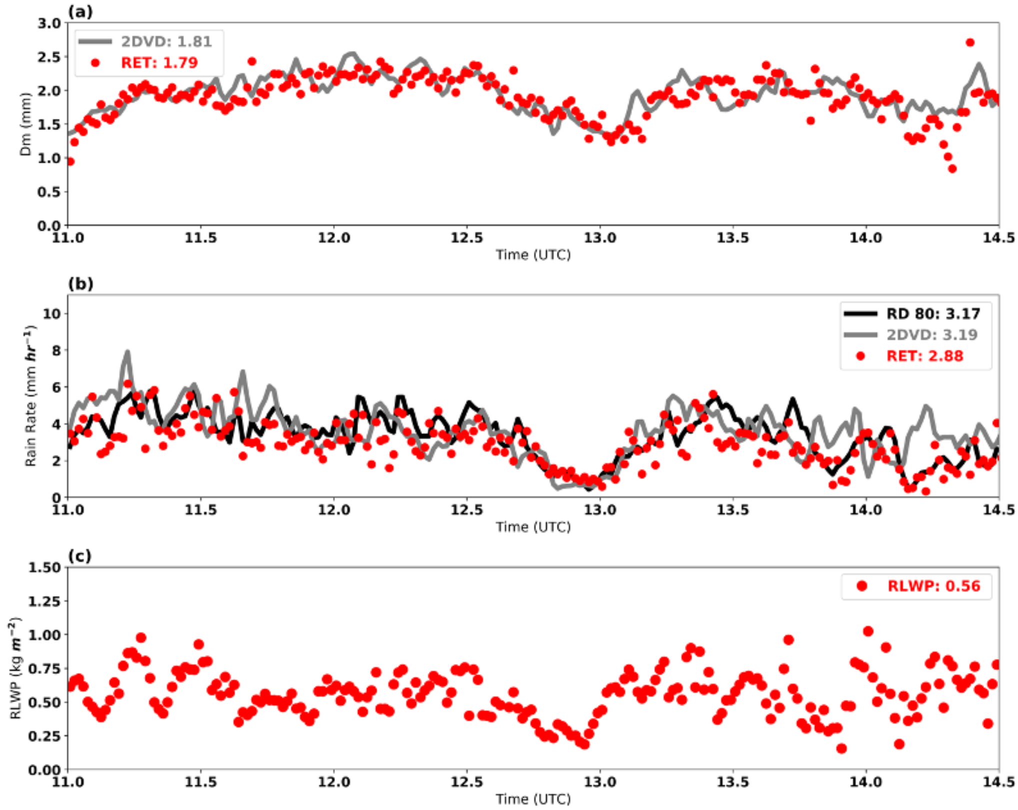

Figure 4. Time series of (a) retrieved (RET) (red dots) and 2DVD surface disdrometer estimated (grey line) D_m, (b) RET (red dots), 2DVD (grey line) and RD-80 (black line) surface disdrometer rain rate estimates, and (c) retrieved rain liquid water path (RLWP, red dots) for Case A (May 20, 2011.

Atmos. Meas. Tech. Discuss., https://doi.org/10.5194/amt-2018-388
Manuscript under review for journal Atmos. Meas. Tech.
Discussion started: 24 January 2019

Atmospheric Measurement Techniques
Discussions

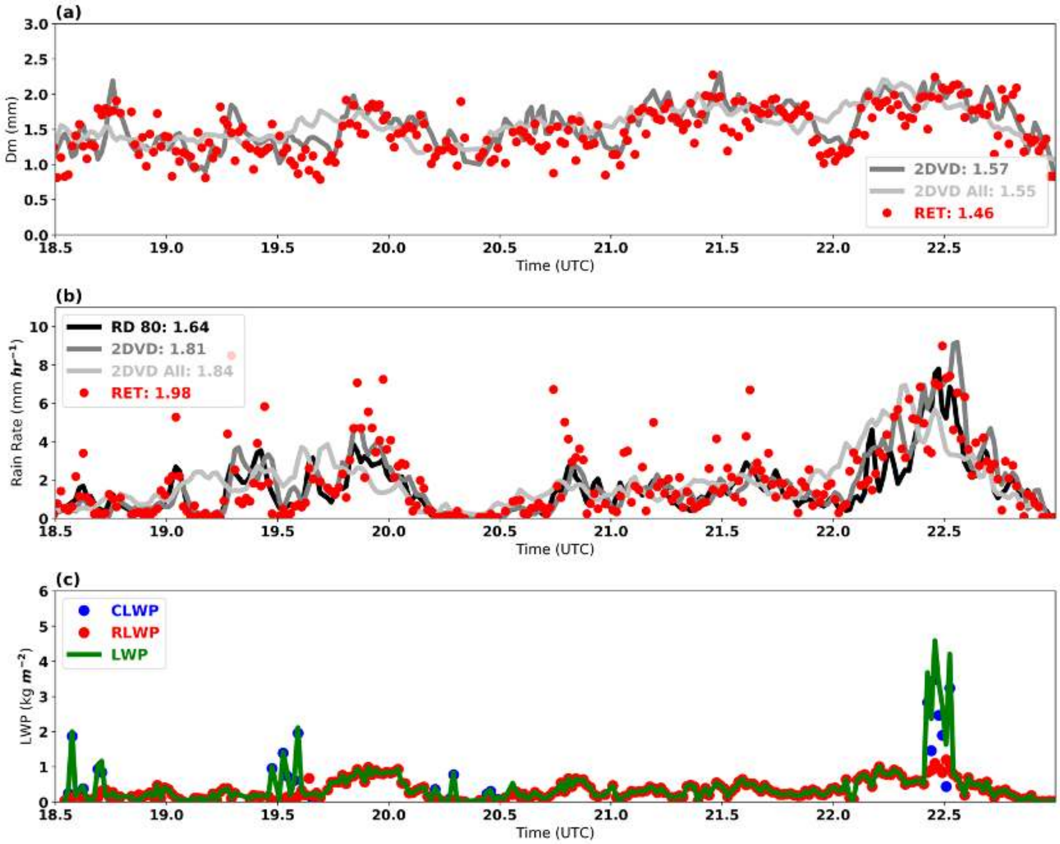

Figure 5. Time series of (a) retrieved (RET) (red dots) and 2DVD surface disdrometer estimated (grey lines) D_m, (b) RET (red dots), 2DVD (grey line) and RD-80 (black line) surface disdrometer rain rate estimates, and (c) rain liquid water path (RLWP, red dots), cloud liquid water path (CLWP, blue dots) and liquid water path (LWP = RLWP+CLWP, green lines) for Case B (May 11, 2011).

Atmos. Meas. Tech. Discuss., https://doi.org/10.5194/amt-2018-388
Manuscript under review for journal Atmos. Meas. Tech.
Discussion started: 24 January 2019

Atmospheric Measurement Techniques
Open Access
Discussions

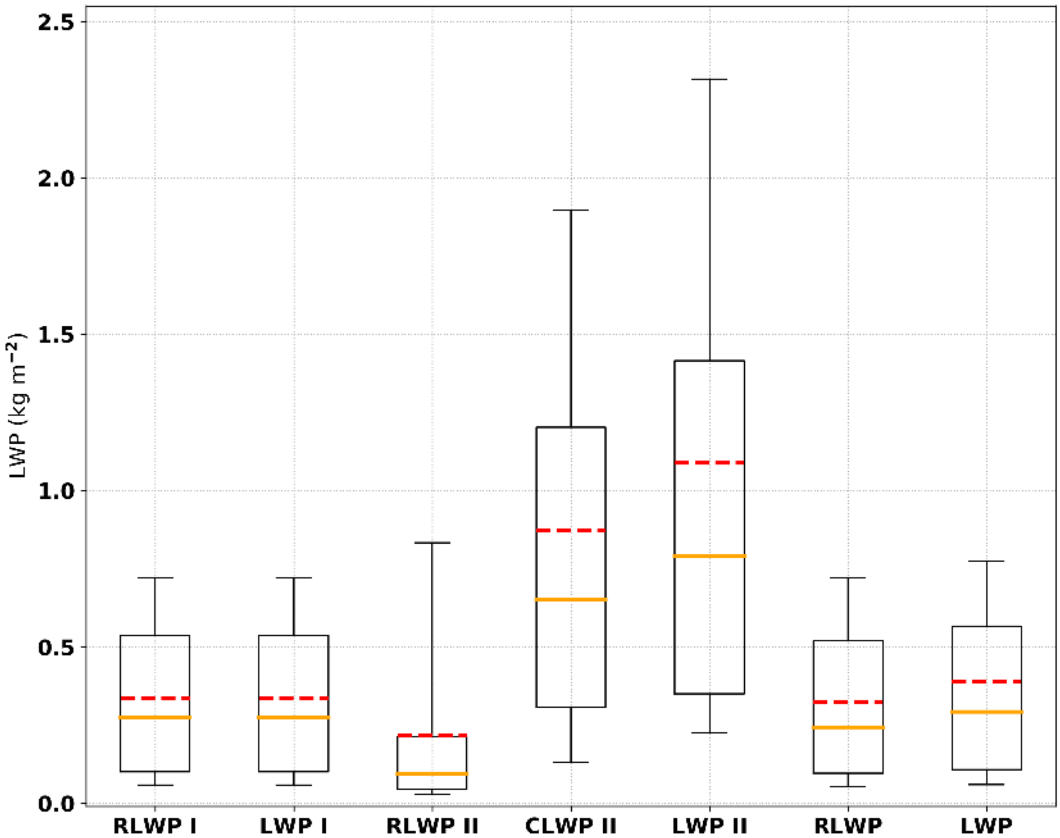

Figure 6. Box and whisker plots of retrieved RLWP, CLWP and LWP for situation (I), (II) and all samples. The horizontal orange line within the box indicates the median, boundaries of the box indicate the 25th- and 75th -percentile, and the whiskers indicate the 10th- and 90th -percentile values of the results. The red dash lines indicate the mean values.

Atmos. Meas. Tech. Discuss., https://doi.org/10.5194/amt-2018-388
Manuscript under review for journal Atmos. Meas. Tech.
Discussion started: 24 January 2019

Atmospheric Measurement Techniques Discussions

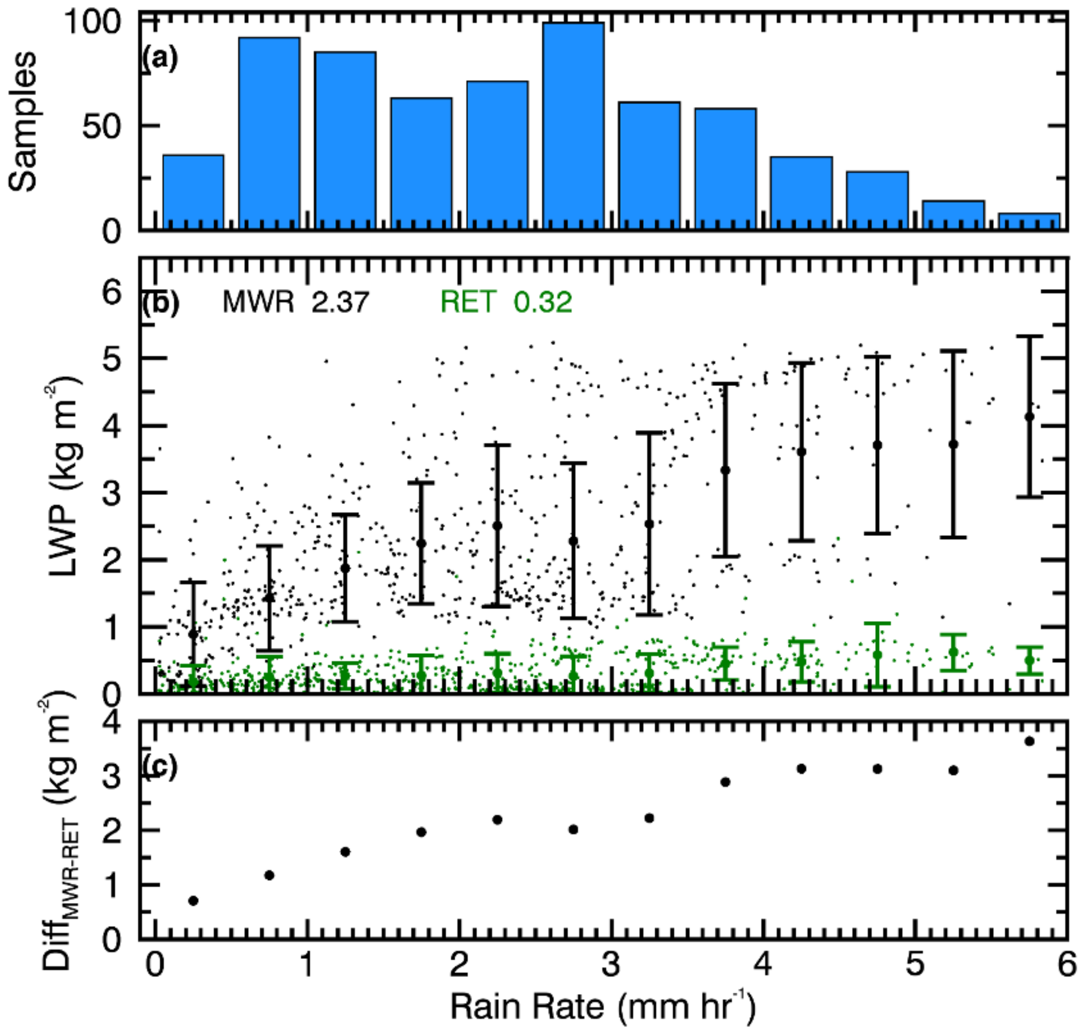

Figure 7. (b) Statistic comparisons between LWP retrievals from this study (RET, dots with one standard deviation bars in green) and microwave radiometer (MWR, black dots with one standard deviation bars in black), (a) corresponding sample numbers (blue bars) in each rain rate bin (0.25 mm hr^{-1}), and (c) the LWP differences between two estimations, shown as a function of rain rate for all cases.

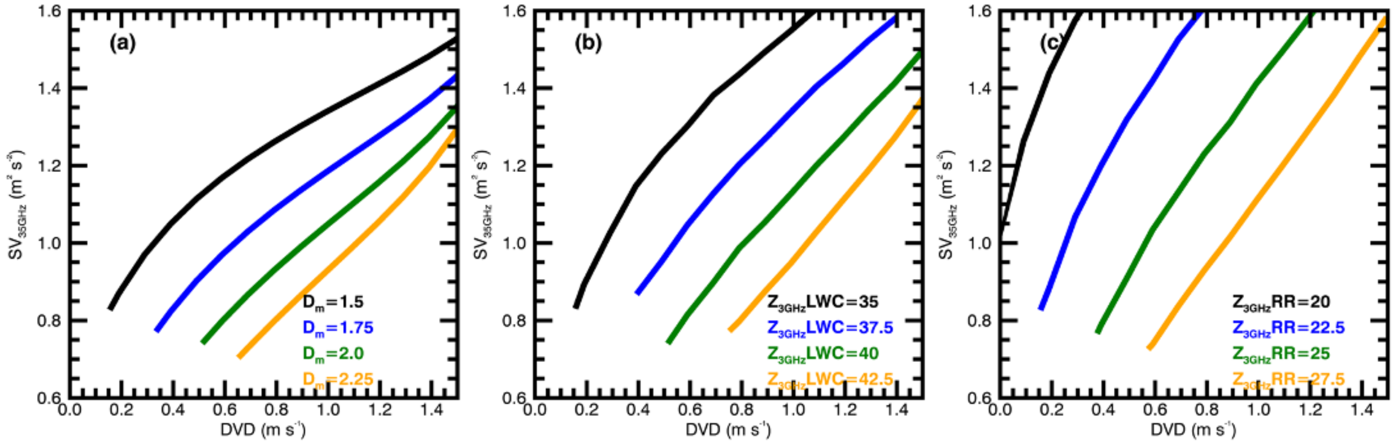

Figure A. Comparisons of (a) mass-weighted mean diameter D_m (mm), (b) parameter $Z_{3GHz}LWC = 10\log(Z_{3GHz}/LWC)$ (dB), and (c) parameter $Z_{3GHz}PR = 10\log(Z_{3GHz}/RR)$ (dB) calculated as functions of Doppler velocity difference (DVD) and spectrum variance at 35 GHz (SV_{35GHz}).